ADVANCED FUNCTIONAL MATERIALS

www.afm-journal.de

Fluorous Metal–Organic Frameworks and Nonporous Coordination Polymers as Low-κ Dielectrics

Simona Galli, Alessandro Cimino, Joshua F. Ivy, Carlotta Giacobbe, Ravi K. Arvapally, Rebecca Vismara, Stefano Checchia, Mustafa A. Rawshdeh, Christian T. Cardenas, Waleed K. Yaseen, Angelo Maspero, and Mohammad A. Omary**

A fluorous metal–organic framework [Cu(FBTB)(DMF)] (FMOF-3) [H_2FBTB = 1,4-bis(1-*H*-tetrazol-5-yl)tetrafluorobenzene] and fluorous nonporous coordination polymer [Ag_2(FBTB)] (FN-PCP-1) are synthesized and characterized as for their structural, thermal, and textural properties. Together with the corresponding nonfluorinated analogues lc-[Cu(BTB)(DMF)] and [Ag_2(BTB)], and two known (super)hydrophobic MOFs, FMOF-1 and ZIF-8, they have been investigated as low-dielectric constant (low-κ) materials under dry and humid conditions. The results show that substitution of hydrogen with fluorine or fluoroalkyl groups on the organic linker imparts higher hydrophobicity and lower polarizability to the overall material. Pellets of FMOF-1, FMOF-3, and FN-PCP-1 exhibit κ values of 1.63(1), 2.44(3), and 2.57(3) at 2×10^6 Hz, respectively, under ambient conditions, versus 2.94(8) and 3.79(1) for lc-[Cu(BTB)(DMF)] and [Ag_2(BTB)], respectively. Such low-κ values persist even upon exposure to almost saturated humidity levels. Correcting for the experimental pellet density, the intrinsic κ for FMOF-1 reaches the remarkably low value of 1.28, the lowest value known to date for a hydrophobic material.

1. Introduction

Due to the increased demand for transistors with decreased size and higher speed, integrated circuits (ICs) have been progressively improved.[1–5] Typical IC mean size is on the 10 nm order of magnitude, which has allowed an increase in microprocessor working frequency to THz levels. Accompanying this increase in speed are limiting factors at the conductor–insulator interconnects, such as signal propagation delay, power dissipation, and cross-talk noise, which limit ultralarge-scale integration of ICs. A turning point to overcome these drawbacks was the switch from aluminum to copper, first realized in a product by IBM in 1997.[6] The next major step forward was the replacement of silica [dielectric constant (κ) ≈ 3.9–4.5[3] depending on the deposition and processing methods] with materials showing lower κ. The International Technology Roadmap for Semiconductors (ITRS)[7] set the κ value of low-κ[8] materials for future chip generations beyond 2016 in the range 2.1–2.5.

In recent years, the quest for low-κ materials as insulators in ICs has focused on inorganic compounds having bonds of lower polarizability than Si—O bonds and/or lower density than silica (2.2–2.4 g cm^{-3}). Replacement of Si—O bonds with Si—F bonds, as in fluorinated silica glasses, led in 2000 to the introduction of the first low-κ material into an IC. Overall, fluorinated silica glasses have shown κ values around 3.6.[1] Substitution of silica Si—O bonds with Si—C bonds, yielding silicon oxycarbides (SiOC:H), has resulted in a significant lowering of κ (e.g., down to 2.8 at 10^6 Hz for PECVD-deposited SiOC:H thin films[9,10]). Fluorinated organic materials have been tested as well: C—F bonds have lower polarizability (0.56 Å^3) and higher energy (485 kJ mol^{-1}) than C—H bonds (0.65 Å^3 and 414 kJ mol^{-1}, respectively).[2] Thus, Teflon-like materials can, in principle, exhibit lower dielectric constant and somewhat higher (albeit still inadequate) thermal stability; for example, polytetrafluoroethylene shows κ values as low as 1.9.[11]

Advantages are conveyed to an insulator also by porosity. The main components of air, N_2, and O_2, are nonpolar, hence the dielectric constant of air is, to a first approximation, equal to

---

Prof. S. Galli, Dr. A. Cimino, R. Vismara, Prof. A. Maspero
Dipartimento di Scienza e Alta Tecnologia
Università dell'Insubria
Via Valleggio 11, 22100 Como, Italy
E-mail: simona.galli@uninsubria.it
Prof. S. Galli
Consorzio Interuniversitario Nazionale per la Scienza
e Tecnologia dei Materiali
Via Giusti 9, 50121 Firenze, Italy
Dr. A. Cimino, Dr. J. F. Ivy, Dr. R. K. Arvapally, M. A. Rawshdeh,
C. T. Cardenas, Dr. W. K. Yaseen, Prof. M. A. Omary
Department of Chemistry
University of North Texas
Denton, TX 76203, USA
E-mail: Mohammad.Omary@unt.edu
Dr. C. Giacobbe, Dr. S. Checchia
European Synchrotron Radiation Facility
71 avenue des Martyrs, CS 40220, 38043 Grenoble Cedex 9, France
Prof. M. A. Omary
Department of Chemistry
Yarmouk University
Irbid 21163, Jordan

The ORCID identification number(s) for the author(s) of this article can be found under https://doi.org/10.1002/adfm.201904707.

DOI: 10.1002/adfm.201904707

that of a vacuum (=1). Notable results in this context have been obtained with xerogels and aerogels, showing κ values lower than 2.[12,13]

None of the classes of insulators quoted above is immune to drawbacks. To be processed, an IC must show adequate thermal stability and mechanical properties. At the end of Cu-based or Al-based IC processing, devices undergo annealing at temperatures of ≈350 °C or 400–450 °C, respectively, under forming gas (N_2:H_2 = 1:9 v/v). While inorganic compounds generally meet these stability requirements (e.g., PECVD-deposited κ-SiOC-0 is stable up to ≈550 °C[14]), organic compounds do not (m.p. of polytetrafluoroethylene = 260 °C). The mechanical properties of amorphous porous dielectrics such as aerogels or xerogels are severely compromised by an increase in porosity,[12,13] raising integration issues with other IC components. Manufacturable solutions are still a challenge.

Recent theoretical and experimental investigations have drawn the attention to nonfluorous[15–29] and fluorous[30] metal–organic frameworks as low-κ materials. Fluorous metal–organic frameworks (FMOFs) and fluorous nonporous coordination polymers (FN-PCPs) are potentially promising alternatives to current low-κ dielectrics, as they possess a number of desirable traits in one material, namely: i) Controlled and reproducible chemical composition; ii) reproducible crystal structure, which allows controlled and reproducible physicochemical properties, which is not always the case with amorphous materials; iii) low adsorptivity of high-κ species. High-κ substances, such as water (κ ≈ 80) and other polar compounds, are produced or present in the environment during IC processing and/or post fabrication. Adsorption of polar compounds dramatically increases κ as observed, e.g., with κ-SiOC-0/1/2.[10] Absence of porosity, as in FN-PCPs, inhibits the adsorption of high-κ compounds. In both FMOFs and FN-PCPs, fluorination promotes an intrinsic increase in hydrophobicity. Despite its permanent porosity, FMOF-1 ($Ag_2[Ag_4Tz_6]$; HTz = 3,5-bis(trifluoromethyl)-1,2,4-triazole, **Scheme 1**), the first fluorous MOF to appear in the literature,[31] is superhydrophobic, as demonstrated by experimental contact angles of 158°.[32]

Recently, three perfluorinated copper(II)-based MOFs have been reported to exhibit hydrophobic behavior with contact angles in the range 108–151°.[33] In principle, superhydrophobic FMOFs allow a platform for further reduction of κ, potentially impeding water to access the pores, hence impeding an increase of the effective κ value.

As demonstrated by previous work of some of us, the exploitation of azolate-[31–39] and poly(azolate)-based[40–44] spacers can afford remarkable thermal stability to MOFs and N-PCPs, often exceeding 400 °C in air.

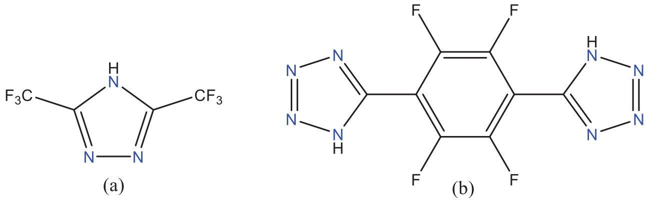

Scheme 1. The molecular structure of a) 3,5-bis(trifluoromethyl)-1,2,4-triazole (HTz), and b) 1,4-bis(1-*H*-tetrazol-5-yl)tetrafluorobenzene (H_2FBTB).

Despite these appealing premises, only few papers regarding MOFs and N-PCPs as low-κ dielectrics have appeared.[15–30] A first point of reference was set by Zagorodniy et al.[15] These authors estimated static dielectric constants as low as 2.0 for a handful of Zn(II)-carboxylate IRMOFs by applying the semiempirical Clausius–Mossotti approach, which neglected the orientation and distortion contributions to the molecular polarizability,[1] influencing the value of κ at the frequencies at which microelectronic chips operate (10^5–10^9 Hz). By first-principle DFT calculations, Warmbier et al.[16] subsequently showed that the κ values reported in[15] were underestimated by less than 10%. As far as it is known,[45–49] promising experimental evidence of κ lower than 2.5 is still infrequent, manifested only by: a) the 2.33(±0.05) value of κ reported[50] for ZIF-8 thin films at 10^5 Hz stored under ambient conditions with estimated ≈60% relative humidity; b) the 2.4 value shown[51] at 10^5 Hz by pellets of [Sr(1,3-BDC)] (1,3-H_2bdc = benzene-1,3-dicarboxylic acid); and c) the 1.2 and 2.1 values reported for films of MOF-3 and MOF-5 at 2×10^6 Hz, respectively.[18] These authors claim that films of MOF-5 are stable if exposed to water vapors, but they do not report κ measurements performed after exposure to humidity. Previous experimental[52,53] and computational[54] pieces of evidence exist for the fact that MOF-5 undergoes a phase change if exposed to moisture.

Within this landscape, FMOF-1 appeared to us an ideal case-study to test the feasibility of FMOFs as low-κ dielectrics. To widen the scope of this investigation, we also focused the attention on a novel FMOF and a novel FN-PCP. We have synthesized for the first time the fluorinated ligand 1,4-bis(1-*H*-tetrazol-5-yl)tetrafluorobenzene (H_2FBTB, Scheme 1) and employed it to build up the Cu(II)-based (FMOF-3) and Ag(I)-based (FN-PCP-1) derivatives isostructural to the already known MOF [Cu(BTB)(DMF)][55] and N-PCP [Ag_2(BTB)][56] (H_2BTB = 1,4-bis(1-*H*-tetrazol-5-yl)benzene[57]), respectively. FMOF-3 represents a more economical choice of the metal center (copper vs silver), as already done by Miljanić and co-workers with extensively fluorinated MOFs (MOFFs),[33,58] whereas FN-PCP-1 provides a platform for comparison upon varying the metal center with the same ligand.

In this work, after briefly summarizing the main structural features, we report on the thermal stability, hydrophobicity, and dielectric properties of FMOF-1, FMOF-3, and FN-PCP-1 in comparison to their nonfluorinated counterparts. The results of high-resolution in situ and operando powder X-ray diffraction studies on FMOF-3 and FN-PCP-1 are also provided to enlighten the structural response of these materials under an AC current of increasing frequency. Overall, these case-studies demonstrate that FMOFs and FN-PCPs show a significant potential as promising novel classes of low-κ dielectrics.

2. Results and Discussion

2.1. Synthesis

FMOF-1 was synthesized by following the previously reported[34] procedure. The fluorinated ligand H_2FBTB (Scheme 1) was prepared for the first time by applying the so-called Demko–Sharpless protocol.[59] The reader is referred to Sections S5 and S6 of the Supporting Information for a detailed description of the synthesis and crystal structure of the ligand. Contrary to [Cu(BTB)(DMF)], the isolation of which requires a strict control of acidity and temperature,[55] FMOF-3·DMF was prepared in a straightforward manner (4 h, 90% yield) in DMF by using copper(II) acetate as the source of metal ions. The choice of the metal(II) salt is crucial for the development of the reaction. The acidity of H_2FBTB is due to the presence of the N-H functionality[60] and is modulated by the electron withdrawing effect of the fluorine atoms on the phenyl ring. The acetate anion is sufficiently basic to deprotonate both tetrazole rings, generating $FBTB^{2-}$ in situ without the need for an extra base. Finally, FN-PCP-1 was isolated by reacting H_2FBTB with silver(I) nitrate in water at reflux. As H_2FBTB is soluble in aqueous solutions, its reaction with $AgNO_3$ proceeds easily in 4 h with a yield amounting to 90%.

2.2. Crystal Structure Analysis

For the sake of comprehension of the subsequent sections, the reader is provided with a brief description of the main structural features of FMOF-1, FMOF-3, and FN-PCP-1. The tetragonal crystal structure of FMOF-1 comprises AgN_3 and Ag_4N_{12} nodes (**Figure 1**a) and μ_3-Tz^- linkers within a 3D porous network possessing 1D hexagonal channels running along the *a*- and *b*-axes (Figure 1b) and having an aperture of ≈0.5 nm.[61] The walls of the channels are decorated by CF_3 groups, which impart hydrophobic character to the pores and, consequently, to the overall material (see below). Toroid-shaped cavities are present within the walls surrounding the channels. At 100 K, even though the void volume amounts to 43%[62] of the unit cell volume, the calculated density (d_c) is rather high (1.76 kg L^{-1}).[39]

FN-PCP-1, isostructural to $[Ag_2(BTB)]$,[56] is built up of tetrahedral AgN_4 nodes (**Figure 2**a) and μ_8-$FBTB^{2-}$ spacers. Overall,

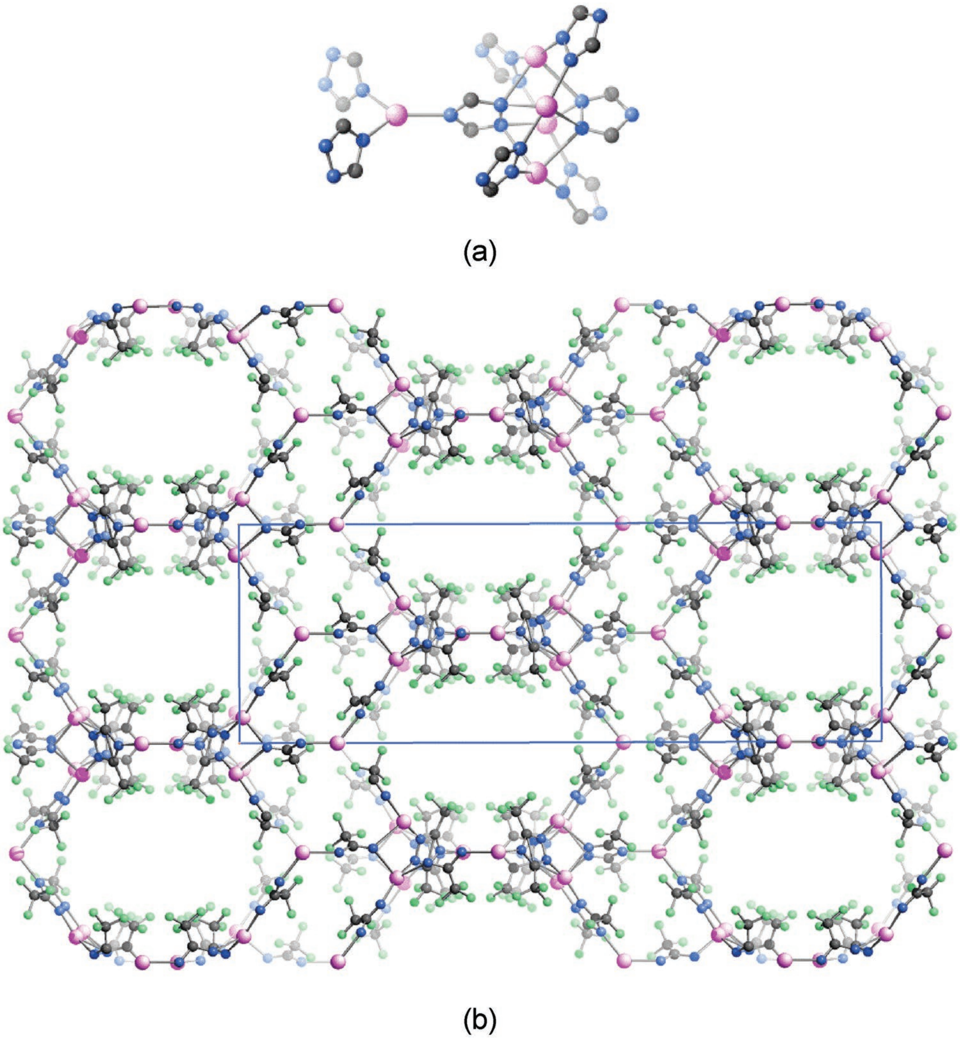

Figure 1. Representation of the crystal structure of FMOF-1. a) The AgN_3 and Ag_4N_{12} nodes (the CF_3 groups have been omitted for clarity). b) Portion of the crystal packing viewed along the [100] direction. The 1D hexagonal channels running parallel to the [100] direction and the toroid-shaped cages can be easily visualized. Horizontal axis, *c*; vertical axis, *b*. Carbon, gray; fluorine, light green; nitrogen, blue; silver, fuchsia.

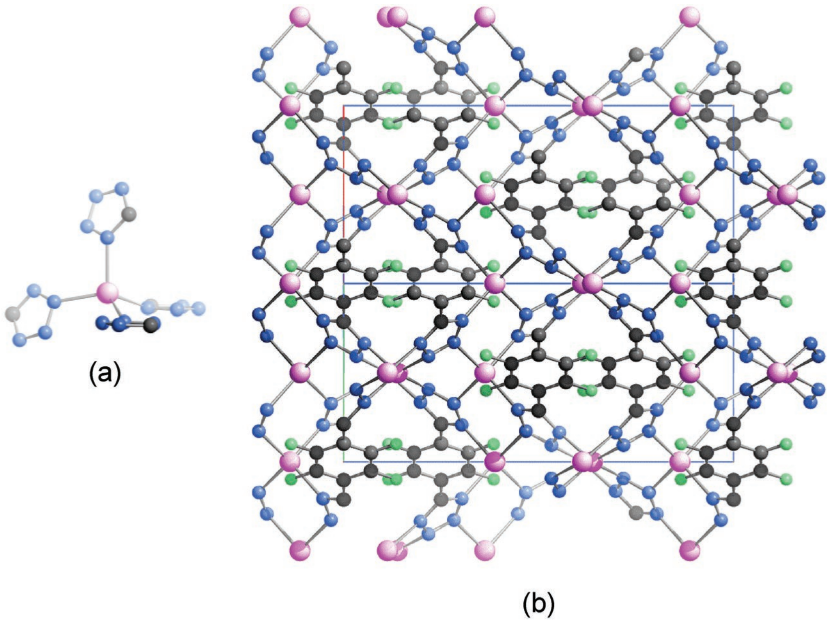

Figure 2. Representation of the crystal structure of FN-PCP-1. a) The tetrahedral AgN_4 node. b) Portion of the crystal packing viewed, in perspective, along the [011] direction. Horizontal axis, *a*. Carbon, gray; fluorine, light green; nitrogen, blue; silver, fuchsia. For a representation along the [010] direction, the reader is addressed to Figure S1 (Supporting Information).

it is a (4,8)-connected nonporous and dense (d_c = 2.94 kg L^{-1}) network, with a rather complex 3D architecture (Figure 2b; Figure S1, Supporting Information). Absence of porosity was confirmed by N_2 adsorption measurements at 77 K and up to 1 bar (Figure S2a, Supporting Information), which revealed a Brunauer, Emmet, and Teller (BET) specific surface area of only 6.4 m^2 g^{-1}.

FMOF-3, exhibiting the same structural motif of [Cu(BTB)(DMF)][55] and [Cu(4-2H$^+$)(H_2O)] [4 = 1,1′-bis(tetrazol-5-yl)tetrafluorobiphenyl],[33] shows an orthorhombic (4,4)-connected 3D network in which 1D chains of *trans*-CuN_4O_2 octahedral nodes (**Figure 3**a) and μ_4-FBTB^{2-} spacers define the vertices and walls, respectively, of 1D rhombic channels (Figure 3b; d_c = 1.77 kg L^{-1}). As in the case of [Cu(BTB)(DMF)], also in FMOF-3,DMF is bound to the metal centers and is not completely removed by thermal activation under vacuum (PXRD evidence). Incidentally, the rather small value (≈62 m^2 g^{-1}) of the BET specific surface area (SSA) retrieved by N_2 adsorption measurements at 77 K (Figure S2a, Supporting Information) suggests the presence of a closed-pore form under these conditions, an occurrence already observed with [Cu(BTB)(DMF)][55] as well as with other MOFs.[63–67] The BET specific surface area could be estimated from the CO_2 adsorption isotherm measured at 273 K as 183 m^2 g^{-1} (Figure S2b, Supporting Information). Finally, calculations with Materials Studio[68] on the ambient-temperature structural model of FMOF-3 yielded an SSA of ≈780 m^2 g^{-1}. This temperature-dependent dynamic pore opening/closure certainly deserves further investigations that, nonetheless, are out of the scope of this work.

2.3. Thermal Stability

The thermal behavior of FMOF-1, FN-PCP-1, and FMOF-3 was investigated by coupling thermal analysis, performed under a flow of N_2, to in situ variable-temperature PXRD (VT-PXRD), carried out in air. The main results are depicted in **Figure 4** and Figures S3 and S4 of the Supporting Information, whereas numeric parameters are collectively provided in **Table 1**. Thin-film assessment under forming gas conditions has not yet been pursued at this fundamental stage of our investigation (see, in this respect, the Conclusion section).

As previously assessed by thermogravimetric analysis (TGA),[38] FMOF-1 is stable under N_2 up to 400 °C. Besides confirming this evidence, VT-PXRD (Figure 4a) shows that neither loss of crystallinity nor phase transitions occur before decomposition. A parametric Le Bail refinement of the VT-PXRD data in the temperature range 30–390 °C (Figure 4b) reveal anisotropic thermal expansion: While the *a*-axis increases by 1.8% with a

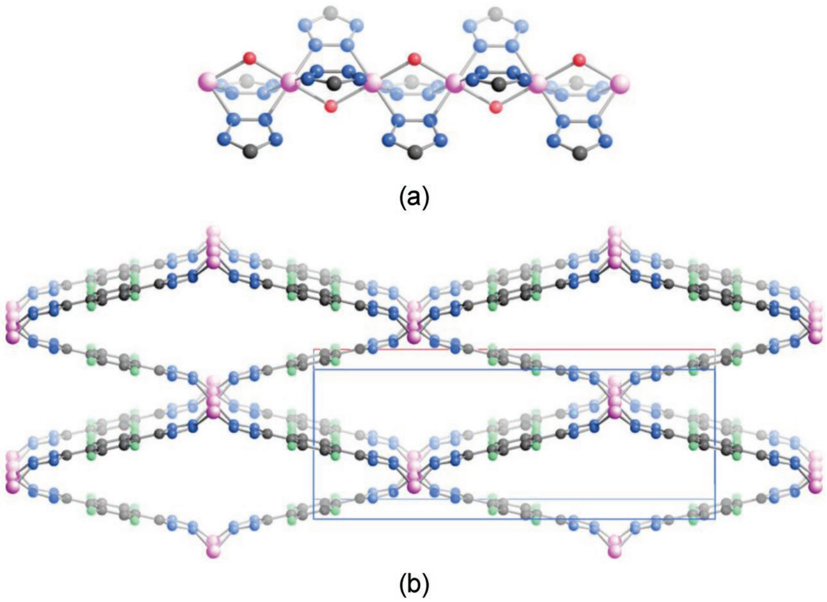

Figure 3. Representation of the crystal structure of FMOF-3. a) Portion of the 1D chain of *trans*-CuN_4O_2 nodes running along the [100] direction. b) Portion of the crystal packing viewed, in perspective, along the [100] direction. An ordered model for the ligand has been used and the DMF molecules [but the oxygen atoms in (a)] have been removed for clarity. Horizontal axis, *b*; vertical axis, *c*. Carbon, gray; copper, fuchsia; fluorine, light green; nitrogen, blue; oxygen, red; sliver, fuchsia.

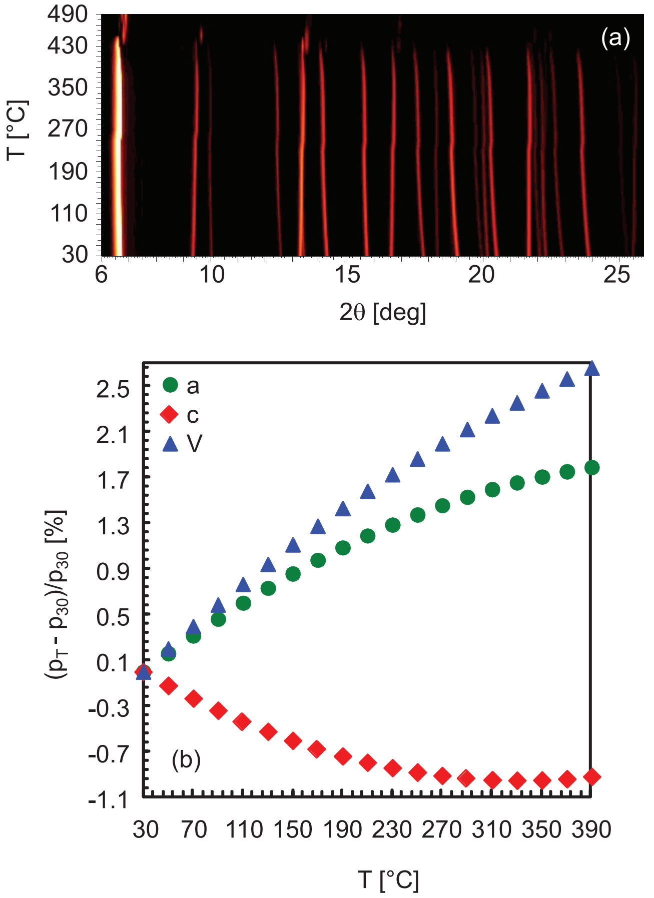

Figure 4. Thermal behavior of FMOF-1. a) Plot of the powder X-ray diffraction patterns measured in situ versus temperature while heating in air in 20 °C steps within the temperature range 30–490 °C. b) Percentage variation of the unit cell parameters (p_T) versus temperature. At each temperature, the values (p_T) have been normalized versus those at 30 °C (p_{30}). *a*, green circles; *c*, red diamonds; *V*, blue triangles.

rate ($\partial a/\partial T$) of 7.0×10^{-4} Å°C^{-1}, the *c*-axis decreases by 0.9% with a rate ($\partial c/\partial T$) of 9.7×10^{-4} Å°C^{-1}, which implies a slight modification of the aperture of the 1D channels running parallel to the [100] direction. Overall, the unit cell volume increases by 2.7%, which corresponds to a coefficient of thermal expansion (CTE) of 7.4×10^{-5} °C^{-1} in this temperature range (lower than the 100 ppm°C^{-1} limit for IC integration).[69]

Table 1. Decomposition temperatures, variation rates of the unit cell axes versus temperature and volumetric coefficients of thermal expansion (CTEs) for FMOF-1, FN-PCP-1, and FMOF-3·DMF.

	T_{dec} [°C]	($\partial a/\partial T$) [Å°C^{-1}]	($\partial b/\partial T$) [Å°C^{-1}]	($\partial V/\partial T$) [Å^3°C^{-1}]	CTE [°C^{-1}]
FMOF-1$^{a)}$	400	7.0×10^{-4}	7.0×10^{-4}	9.7×10^{-4}	7.4×10^{-5}
FN-PCP-1$^{b)}$	400	8.0×10^{-5}	6.0×10^{-5}	4.5×10^{-4}	4.7×10^{-5}
FMOF-3·DMF$^{c)}$	260	-2.0×10^{-5}	-3.2×10^{-4}	4.9×10^{-4}	3.7×10^{-5}

Variation rates and CTEs estimated in the range: $^{a)}$30–390 °C; $^{b)}$30–350 °C; $^{c)}$30–240 °C.

FN-PCP-1 is stable under N_2 up to 360 °C (Figure S3a, Supporting Information). A parametric Le Bail treatment of the VT-PXRD data acquired in the range 30–350 °C (Figure S3b,c, Supporting Information) highlights that, while the *a*- and *b*-axes vary negligibly (less than 0.2%; $\partial a/\partial T = 8.0 \times 10^{-5}$ Å°C^{-1}, $\partial b/\partial T = 6.0 \times 10^{-5}$ Å°C^{-1}), the *c*-axis increases by about 1.6% ($\partial c/\partial T = 4.5 \times 10^{-4}$ Å°C^{-1}), implying an overall volumetric thermal expansion of 1.6% (CTE = 4.7×10^{-5} °C^{-1}). FMOF-3 is stable up to only 270 °C, both under N_2 and in air (Figure S4a,b, Supporting Information). The ≈4 wt% loss observed (Figure S4a, Supporting Information) in the temperature range 50–140 °C can be ascribed to the loss of clathrated DMF molecules (0.25 mol of DMF per formula unit; theoretical loss 4.2 wt%). Notably, the nonfluorinated analogue [Cu(BTB)(DMF)] is less stable, as it undergoes a phase transition to a low-crystallinity phase already at 100 °C.[55] A parametric Le Bail refinement of the VT-PXRD data acquired in the temperature range 30–250 °C disclosed a 0.8% expansion of the unit cell volume (Figure S4c, Supporting Information),[70] with a CTE of 3.7×10^{-5} °C^{-1}. The *a*-axis is almost unaffected by temperature increase ($\partial a/\partial T = -2.0 \times 10^{-5}$ Å°C^{-1}) while the *b*- and *c*-axis, the diagonals of the rhombic channels, vary by −0.3% and 1.2% ($\partial b/\partial T = -3.2 \times 10^{-4}$ Å°C^{-1}, $\partial c/\partial T = 4.9 \times 10^{-4}$ Å°C^{-1}), respectively. This implies a slight modification[71] of the aperture of the channels.

2.4. Hydrophobicity

FMOF-1 is superhydrophobic,[32] showing experimental contact angles near 160°. Contrary to the prototypical adsorbents BPL carbon and zeolite-5A, it does not adsorb water up to 95% relative humidity.[38] Finally, it is stable if exposed to water vapor at room temperature for at least 70 d (**Figure 5**). Since pressing this MOF into pellets to measure the dielectric constant brings about amorphization, we also monitored a pellet of FMOF-1 exposed to water vapor at room temperature: The pellet is stable for at least 70 d (Figure S5, Supporting Information). These observations prove that, despite having hexagonal channels wider than the kinetic diameter of water (2.6 Å[72]), FMOF-1 displays extraordinary hydrophobicity.

To gain preliminary insights on the hydrophobicity of FN-PCP-1, we measured its contact angle and monitored its stability versus water vapor, as detailed in the Experimental Section. This material shows an experimental contact angle of ≈75°, to be compared to the value of ≈55° of the nonfluorinated counterpart (**Figure 6**). Moreover, it is stable at least up to 48 d if exposed to water vapor at ambient temperature (Figure S6a, Supporting Information), whereas FMOF-3 is not as stable under the same conditions (Figure S6b, Supporting Information), though its contact angle is ≈86° (Figure S7, Supporting Information).[73]

The hydrophobic behavior of the materials herein is attributed to the fluorination of the ligands bonded to the Cu(II) or Ag(I) centers. Whilst we are cognizant about copper and silver being problematic for silicon-based IC devices, we have not experienced any metallization of the copper(II) or silver(I) ions of the title compounds on extended storage under ambient conditions, at elevated temperatures, or even under extended UV irradiation–perhaps due to a “Teflon coating” influence of the fluorinated ligands on the metal centers.

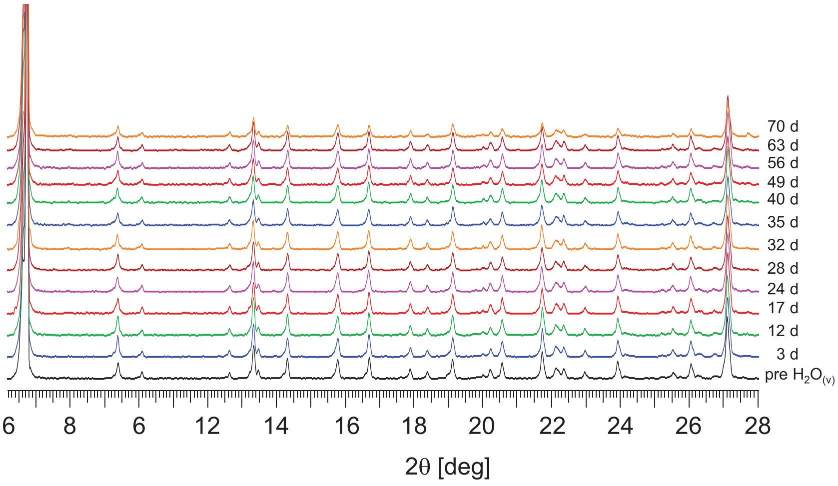

Figure 5. PXRD monitoring of a powdered sample of FMOF-1 exposed to water vapor at ambient temperature (a magnified version can be seen in Figure S8 of the Supporting Information).

2.5. Measurement of the Dielectric Constant

The value of the dielectric constant for H_2FBTB, FMOF-1, FN-PCP-1, and FMOF-3 pressed into pellets was assessed at room temperature by metal–insulator–metal parallel plate capacitance measurements at 2 V and in the frequency range 2 Hz -2×10^6 Hz. The results described below are collected in **Table 2** while the curves depicting the behavior of κ versus frequency are reported in **Figure 7** and Figure S9 (Supporting Information). The positive effect of fluorination is evident already in the case of the ligands: At 2×10^6 Hz, H_2FBTB and H_2BTB show average κ values of 2.55(2) and 4.17(1), respectively (Figure S9, Supporting Information). This trend is maintained also in the case of the fluorinated and nonfluorinated coordination frameworks: FN-PCP-1 shows an average value of κ of 2.57(3) versus the average value of 3.79(1) for $[Ag_2(BTB)]$ (best values 2.53 and 3.78, respectively). FMOF-3 shows average and best values of κ of 2.44(3) and 2.36, respectively, in comparison with the values of 2.94(8) and 2.85 of lc-[Cu(BTB)(DMF)]. Both FN-PCP-1 and FMOF-3 could, therefore, be used for 10 nm technology nodes.[1]

According to recent ITRS Roadmap reports, manufacturable solutions exist and are being optimized for materials with κ in the range 2.6–3.0, and are known for materials with κ in the range 2.4–2.8.[1]

FMOF-1 shows average κ values of 1.89(1) (best value 1.89) and 1.63(1) (best value 1.63) when pressed at 0.5 and 0.7 kbar, respectively. This remarkable result demonstrates that FMOFs can in principle be used as low-κ materials for technology nodes below 7 nm.[1] Moreover, this result confirms the higher effectiveness of CF_3 groups in conferring hydrophobicity versus direct fluorination on the skeleton of the ligand, as already observed with the $Ni_8(OH)_4(H_2O)_2(L)_6$ [L = bis(pyrazolate) ligand] MOFs.[74]

To consider the air gaps reasonably present in the pellets, we measured the pellet density by pycnometry (**Table 3**) and corrected the observed values of κ by applying the parallel medium approximation to calculate the κ values corresponding to the bulk (Table 3, κ_{corr}). As for FMOF-1 pressed at 0.7 kbar, the intrinsic κ reaches the remarkably low value of 1.28, which as far as it is known, is the lowest κ values ever reported for a hydrophobic material, witnessing that FMOFs can be platforms for ultralow-κ properties.[76]

To test the performance of FN-PCP-1, FMOF-3, and FMOF-1 against water vapor when pressed into pellets, we also estimated the dielectric constant after placing the pellets of the three compounds for 24 h in an air-tight cell at nearly saturated humidity levels. The materials show only a slight increase of κ, reaching average values of 2.64(4), 2.51(3), and 2.11(1), respectively, at 2×10^6 Hz. Toward practical use, however, we caution that thin films, where the surface to volume ratio is much higher, may afford lower resistance to humidity.

To put these measurements into perspective with a standard hydrophobic MOF, we measured the dielectric constant of a pellet of ZIF-8,[77] which has a contact angle of ≈56°,[78] under conditions similar to those adopted for the other materials herein. The average and best values obtained at room temperature and 2×10^6 Hz previous to exposure to water vapors [1.95(3) and 1.91, respectively] can be only indirectly compared versus those of Eslava and co-workers,[50] who performed their measurements on an in situ grown thin film at 60% RH to attain κ = 2.33 at 100 kHz. Additionally, pressing ZIF-8 into pellets brings about partial amorphization (PXRD evidence; see Figure S10, Supporting Information). The measurements on amorphous ZIF-8, nevertheless, remain useful to calibrate the dielectric properties for different hydrophobic chemical compositions. After exposing a pellet of ZIF-8 to water vapor for 24 h, at 2×10^6 Hz the κ magnitude started at 5.90, then progressively decreased to 2.00 along consecutive measurements (Figure S11, Supporting Information). This behavior likely suggests that the water adsorbed onto the surface of the pellet is progressively released, whereas the initial drastic elevation upon nearly saturated RH is consistent with the type-3 H_2O adsorption isotherm at RH > 80% reported in ref. [50] In the case of FN-PCP-1, FMOF-3, and FMOF-1, the five consecutive repetitions

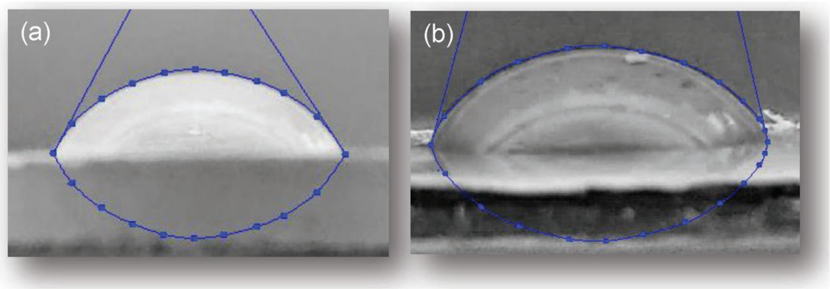

Figure 6. Estimation of the contact angle for a) $[Ag_2(BTB)]$ and b) FN-PCP-1.

Table 2. Values of κ at 2 V and 2×10^6 Hz for FMOF-1 (pressed at 0.5 and 0.7 kbar), FN-PCP-1, [Ag_2(BTB)], FMOF-3, lc-[Cu(BTB)(DMF)], and ZIF-8 under ambient and near saturated humidity levels.

Compound	κ at 2×10^6 Hz (ambient RH)	κ at 2×10^6 Hz (≈saturated RH)
FMOF-1, batch 1[a)]	1.89(1) [1.63(1)]	n.a.
FMOF-1, batch 2	2.00(1)	2.11(1)
FN-PCP-1	2.57(3)	2.64(4)
[Ag_2(BTB)]	3.79(1)	n.a.
FMOF-3	2.44(3)	2.51(3)
lc-[Cu(BTB)(DMF)]	2.94(8)	n.a.
ZIF-8	1.95(3)	5.90

[a)] Values for a pellet pressed at 0.7 kbar are in square brackets.[75]

yielded almost superimposable values (Figure S11, Supporting Information).

We have performed preliminary film-casting studies for FMOF-1 as we have discovered that, counterintuitively versus the normal behavior of MOFs and CPs, it can dissolve and recrystallize upon casting on a solid support from solutions of certain organic solvents. However, such thin films did not contain the desired FMOF-1 phase (see Figure S12, Supporting Information). Additionally, from visual inspection, they seemed not to be contiguous. Thicker films (≈40 µm) with better uniformity were successfully cast on silicon upon tuning deposition conditions (e.g., varying the concentration, temperature, and/or solvent composition). However, these films did not contain the same phase as that of FMOF-1, either (Figure S12, Supporting Information). We have not pursued κ measurements for these thin and thick films, pending both the optimization of deposition of contiguous films of the former, and the phase identification in both cases.

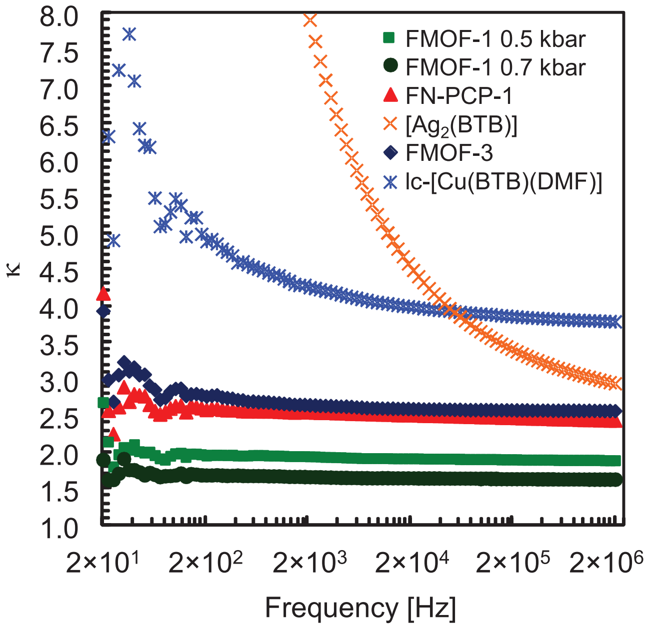

Figure 7. Variation of κ as a function of frequency at 2 V for FMOF-1 (pressed at 0.5 and 0.7 kbar), FN-PCP-1, [Ag_2(BTB)], FMOF-3, and lc-[Cu(BTB)(DMF)].

Table 3. Bulk and pellet densities and observed and corrected values of κ at 2 V and 2×10^6 Hz for FMOF-1 (pressed at 0.5 and 0.7 kbar), FN-PCP-1, and FMOF-3.

Compound	κ_{obs}[b)]	d_{pellet} [kg L^{-1}]	d_{bulk} [kg L^{-1}]	κ_{corr}[b)]
FMOF-1[a)]	1.89(1) [1.63(1)]	1.59 [2.46]	1.76	2.24 [1.28]
FN-PCP-1	2.57(3)	1.88	2.94	4.97
FMOF-3	2.44(3)	1.57	1.77	3.20

[a)] Values for a pellet pressed at 0.7 kbar are in square brackets; [b)] at 2×10^6 Hz and ambient RH.

2.6. High-Resolution PXRD

Visual inspection of the HR-PXRD data acquired on pellets of FN-PCP-1 and FMOF-3 (Figure S13, Supporting Information) clearly suggested that the structural features of the two compounds are not affected by the passage of an AC current with increasing frequency in the range 0–5×10^5 Hz. To support this qualitative observation, Rietveld refinements were carried out on selected HR-PXRD data. Figure S14 of the Supporting Information provides representative examples of the final stage of the Rietveld refinements, whereas Table S1 of the Supporting Information collects the main crystallographic details retrieved from all the data. As is evident from Table S1 of the Supporting Information, the unit cell parameters of FN-PCP-1 and FMOF-3 undergo negligible variations (less than ± 0.1%), well within experimental error, as a function of frequency.

3. Conclusion

Herein, we have demonstrated that fluorinated metal–organic frameworks and fluorinated nonporous coordination polymers show a promising potential as low-κ materials upon further development following this fundamental investigation of their basic electrical, structural, and thermal properties in crystalline forms. Pellets of FMOF-3 and FN-PCP-1, which is stable under water vapor at least for 48 d, show average κ values of 2.44(3) and 2.57(3), respectively, at 2×10^6 Hz under ambient conditions, which increase only modestly–to 2.51(3) and 2.64(4), respectively–after exposure to water vapor at RH conditions near saturation.

Even more promising, after being pressed at 0.7 kbar, FMOF-1, stable under water vapor for at least 70 d, shows pellet κ values of 1.63(1) at 2×10^6 Hz and intrinsic κ values as low as 1.28 at 2×10^6 Hz under ambient conditions, one of the lowest κ values ever reported for a MOF and the lowest for a hydrophobic material. Hence, FMOF-1 shows potential even as an ultralow-κ material. Distinct from FN-PCPs, FMOFs offer a platform for further development of ultralow-κ materials, given the modest surface area of ≈800 m^2 g^{-1} of FMOF-1; hence, additional development of FMOFs with higher surface area while maintaining water stability and superhydrophobicity due to perfluorination should, in principle, offer an opportunity for further reduction in κ values even below 1.28.

Additional investigations of the material compositions herein, as is or upon slight alterations, are warranted to assess the hydrothermal stability under forming gas as well as the mechanical properties in functional forms (i.e., thin films on Ta or W, their nitrides, or Cu).

4. Experimental Section

Materials and Methods: All the solvents and reagents were obtained from commercial suppliers and used without further purification. IR spectra were acquired in attenuated total reflectance on a diamond crystal by means of a Nicolet iS10 instrument over the range 4000–500 cm^{-1}; in the following, band maximum positions were reported in cm^{-1}, while band shapes and intensities are denoted as: b = broad, versus = very strong, s = strong, m = medium, w = weak, and vw = very weak. ^{1}H, ^{13}C(APT) and ^{19}F NMR spectra were recorded at 400, 100, and 376 MHz, respectively, on a Bruker Avance 400 spectrometer in DMSO-d_6. ^{1}H, ^{13}C, and ^{19}F NMR data were reported as follows: Chemical shifts (in ppm, referenced to internal TMS for ^{1}H and ^{13}C and TFA for ^{19}F) and multiplicity (s = singlet, m = multiplet, dm = doublet of multiplets). TGA was performed with a Netzsch STA 409 instrument under a flow of N_2, in the temperature range 30–900 °C and at a heating rate of 10 °C min^{-1}. Elemental analyses were obtained with a Perkin Elmer CHN Analyser 2400 Series II. Powder X-ray diffraction patterns for qualitative analysis prior to functional characterization were acquired in the 3–35° 2θ range, with steps of 0.02° and time/step of 1 s, on a Bruker AXS D8 Advance diffractometer equipped with a Cu-Kα tube (λ = 1.5418 Å), a Bruker Lynxeye linear position-sensitive detector, a filter of nickel in the diffracted beam, and the following optics: Primary beam Soller slits (2.3°), fixed divergence slit (0.5°), receiving slit (8 mm). The generator was set at 40 kV and 40 mA.

Synthesis of the H_2FBTB Ligand: The reader is referred to Section S5 of the Supporting Information for details on the synthesis of H_2FBTB and Section S6 (Figure S15 and S16, Supporting Information) for the description of the crystal and molecular structure (CCDC number: 1 824 197).

Synthesis of the NH_4Tz Ligand: NH_4Tz was prepared according to procedures previously reported by Tipping and co-workers for four synthetic steps, with steps 1–2 according to Bell et al.[79] while steps 3–4 according to Abdul-Ghani et al.[80]

Synthesis of the H_2BTB Ligand: H_2BTB was prepared according to a previously published protocol.[56]

Synthesis of $Ag_2[Ag_4Tz_6]$ (FMOF-1): FMOF-1 was isolated in the form of white microcrystalline powders by following a previously reported procedure.[31] Batches of FMOF-1 were verified by comparison of their N_2 adsorption isotherms and PXRD patterns to published ones.

Synthesis of $[Ag_2(BTB)]$: $[Ag_2(BTB)]$ was obtained in the form of brownish microcrystalline powders by following a previously reported procedure.[56] IR (cm^{-1}): 1377 (m), 1278 (m), 1219 (vw), 1157 (m), 1109 (w), 1083 (w), 1039 (w), 1005 (w), 845 (s), 741 (s). Elem. Anal. calc. for $[Ag_2(BTB)]$ (FW = 427.7 g mol^{-1}): C, 22.44; H, 0.94; N, 26.18%; found: C, 23.36; H, 1.16; N, 25.68%.

Synthesis of $[Ag_2(FBTB)]$ (FN-PCP-1): In a Schlenk tube, $AgNO_3$ (0.100 g, 0.35 mmol) was suspended in distilled water (6 mL). After raising the temperature up to 60 °C, H_2FBTB (0.118 g, 0.69 mmol) was added under vigorous stirring. The reaction mixture was refluxed for 4 h under vigorous stirring. A light brown solid was formed. The mixture was allowed to cool down to room temperature and the solid was collected by vacuum filtration, washed with distilled water (10 mL) and methanol (10 mL), and dried under vacuum (100 °C, 10^{-4} bar, 4 h) to afford the title compound as a light brown microcrystalline powder. Yield: 92%. IR (cm^{-1}): 1492 (s), 1481 (s), 1399 (m), 1356 (w), 1258 (w), 1152 (w), 981 (s), 793 (s). Elem. Anal. calc. for $[Ag_2(FBTB)]$ (FW = 499.9 g mol^{-1}): C, 19.22; H, 0.00; N, 22.42%; found: C, 19.63; H, 0.15; N, 22.45%.

Synthesis of lc-$[Cu(BTB)(DMF)]\cdot CH_3OH$: Attempts to obtain [Cu(BTB)(DMF)] in the form of microcrystalline powders by following the procedure adopted by Dincă and co-workers[55] to grow single crystals invariably failed, yielding cyan powders of a low-crystallinity phase (lc-$[Cu(BTB)(DMF)]\cdot CH_3OH$). The latter could be isolated also by following a slightly different path, namely: In a Schlenk tube, H_2BTB (0.100 g, 0.47 mmol) was dissolved in DMF (5 mL). After raising the temperature up to 60 °C, $Cu(OAc)_2$ (0.093 g, 0.47 mmol) was added under vigorous stirring. The reaction mixture was kept at 135 °C for 4 h under vigorous stirring. A bluish precipitate was formed. The mixture was allowed to cool down to room temperature and the solid was collected under vacuum filtration, washed with methanol (10 mL) and dried under vacuum (100 °C, 10^{-4} bar, 4 h) to afford a cyan powder. Yield: 69%. IR (cm^{-1}): 3453 (b), 2933 (w), 2870 (w), 1652 (vs), 1494 (w), 1436 (w), 1403 (w), 1388 (m), 1252 (w), 1096 (m), 1062 (w), 1031 (w), 1007 (w), 853 (w), 739 (w), 663 (w). Elem. Anal. calc. for lc-$[Cu(BTB)(DMF)]\cdot CH_3OH$ (FW = 394.9 g mol^{-1}): C, 39.54; H, 4.34; N, 31.92%; found: C, 38.95; H, 4.78; N, 31.45%. For the measurement of κ, lc-$[Cu(BTB)(DMF)]\cdot CH_3OH$ was activated at 120 °C and 10^{-4} bar for 12 h to remove clathrated CH_3OH.

Synthesis of $[Cu(FBTB)(DMF)]\cdot 0.25DMF$ (FMOF-3·DMF): In a Schlenk tube, H_2FBTB (0.100 g, 0.35 mmol) was dissolved in DMF (5 mL). After raising the temperature up to 60 °C, $Cu(OAc)_2$ (0.069 g, 0.35 mmol) was added under vigorous stirring. The reaction mixture was kept at 135 °C for 4 h under vigorous stirring. A cyan precipitate was formed. The mixture was allowed to cool down to room temperature and the solid was collected by vacuum filtration, washed with methanol (10 mL), and dried under vacuum (100 °C, 10^{-4} bar, 4 h) to afford the title compound as cyan microcrystalline powders. Yield: 90%. IR (cm^{-1}): 1499 (s), 1486 (s), 1417 (w), 1403 (w), 1384 (w), 1356 (vw), 1274 (vw), 1220 (vw), 1105 (w), 1070 (vw), 984 (s), 802 (s), 736 (m), 669 (m). Elem. Anal. calc. for $[Cu(FBTB)(DMF)]\cdot 0.25DMF$ (FW = 439.4 g mol^{-1}): C, 32.14; H, 2.01; N, 29.51%; found: C, 31.82; H, 1.89; N, 30.32%. For the structural characterization, assessment of hydrophobicity, measurement of κ, and high-resolution powder diffraction, FMOF-3·DMF was activated at 120 °C and 10^{-4} bar for 12 h to remove clathrated DMF.

Synthesis of [Zn(MeIm)] (ZIF-8): ZIF-8 was isolated in the form of white microcrystalline powders by following a previously reported synthesis.[78] Zinc nitrate hexahydrate (98%) and 2-methylimidazole (HMeIm) (99%) were purchased from Sigma-Aldrich and used without further purification.

Powder X-ray Diffraction Structural Analysis: Microcrystalline samples of FMOF-3 and FN-PCP-1 were lightly ground with agate mortar and pestle. Then, they were deposited in the hollow of a silicon zero-background plate 0.1 mm deep. After fast preliminary acquisitions in the 2θ range 3–35° for qualitative analysis, diffraction data for structure refinements were collected at room temperature, in the 2θ range 5–105°, with steps of 0.02° and a total scan time of ≈12 h, on the Bruker AXS D8 Advance diffractometer described above. Comparison between the PXRD patterns of FMOF-3 versus [Cu(BTB)(DMF)][55] and FN-PCP-1 versus $[Ag_2(BTB)]$[56] suggested that the two fluorinated compounds are isostructural to the nonfluorinated counterparts. Hence, refinement of the crystal structures of FMOF-3 and FN-PCP-1 were carried out, by applying the Rietveld method[81] as implemented in TOPAS-R,[82] starting from the structural models of [Cu(BTB)(DMF)] and $[Ag_2(BTB)]$, respectively. The independent portion of the $FBTB^{2-}$ ligand and the DMF molecule in FMOF-3 were described through rigid bodies, imposing idealized bond distances and angles.[83] The presence of orientation disorder, with respect to the main axis of the ligand, affecting the phenyl ring in FMOF-3 was verified during the final stages of the refinement and was found beneficial (as proved by the lowering of the figures of merit R_p and R_{wp}). For both compounds, the background was modeled by a polynomial function. A refined, isotropic thermal parameter was assigned to the metal atoms; lighter atoms were assigned an isotropic thermal parameter 2.0 $Å^2$ higher. The peak shapes were described with the fundamental parameters approach.[84] For FN-PCP-1, peak shape anisotropy was described according to the model proposed by Stephens[85] for orthorhombic space groups using Lorentzian and

Gaussian contributions, while in the case of FMOF-3 1/cos(θ)-dependent spherical harmonics were necessary. The final Rietveld refinement plots are supplied in Figure S17 (Supporting Information). Fractional atomic coordinates are provided in the Supporting Information as CIF files.

Main crystallographic details for FN-PCP-1: orthorhombic, *Fddd*, a = 17.2720(4) Å, b = 13.5506(3) Å, c = 9.6507(3) Å, V = 2258.7(1) Å^3, Z = 32, Z' = 8, d_c = 2.94 kg/L, F(000) = 1872, R_{Bragg} = 3.70%, R_p = 4.12%, and R_{wp} = 5.50%, for 4751 data and 37 parameters in the 10–105° (2θ) range. CCDC number: 1 824 198.

Main crystallographic details for FMOF-3: orthorhombic, *Imma*, a = 7.0087(4) Å, b = 24.307(1) Å, c = 9.2770(7) Å, V = 1580.4(2) Å^3, Z = 16, Z' = 4, d_c = 1.77 kg/L, F(000) = 836, R_{Bragg} = 1.20%, R_p = 2.42% and R_{wp} = 3.23%, for 4951 data and 46 parameters in the 6–105° (2θ) range. CCDC number: 1 824 199.

Variable-Temperature Powder X-Ray Diffraction: In situ variable-temperature powder X-ray diffraction (VT-PXRD) experiments were performed on FMOF-1, FMOF-3, and FN-PCP-1. 30 mg samples of the three compounds were ground with agate mortar and pestle and deposited in the hollow of an aluminum sample holder. By means of a custom-made sample heater (Officina Elettrotecnica di Tenno, Ponte Arche, Italy), mounted on the Bruker AXS D8 Advance diffractometer described above, the samples were heated in air from 30 °C up to decomposition, with steps of 20 °C; a PXRD pattern was acquired in isothermal conditions at each step, covering a suitable low-to-medium-angle 2θ range. Treating the data acquired before loss of crystallinity by means of a Le Bail parametric refinement[86] enabled us to investigate the behaviour of the unit cell parameters as a function of the temperature. Note: when comparing the results of TGA and VT-PXRD, the reader must be aware that the thermocouple of the latter set-up is not in direct contact with the sample, this determining a slight difference in the temperature at which the same event is detected by the two techniques. The temperatures deriving from TGA are more reliable.

N_2 Adsorption Measurements: N_2 adsorption isotherms were measured on FN-PCP-1 and FMOF-3 with a standard static volumetric technique at 77 K and up to 1 bar, using a Micromeritics ASAP 2020 accelerated surface area and porosimetry analyzer. FMOF-3·DMF was preliminarily activated under vacuum (120 °C, 10^{-4} bar, 12 h) and stored at ambient conditions. Prior to measurement, the samples were activated in situ by heating at 100 °C under vacuum for 2 h. Specific surface areas were calculated using the BET model.[87]

CO_2 Adsorption Measurement: Adsorption and desorption isotherms were obtained via a TA Instruments Q5000 SA and VTI-SA high sensitivity thermogravimetric dynamic sorption analyzer which enabled sorption analysis of a dry powder sample of FMOF-3 at 273 K by monitoring the weight change of the sample as a function of relative pressure of CO_2. The balance has a signal resolution of 0.01 µg, and a sensitivity of 0.1 µg.

Chemical Stability Tests: To monitor the stability of FMOF-1, FN-PCP-1, and FMOF-3 versus water vapor, 15 mg samples were deposited in the hollow of aluminum sample-holders. Preliminary PXRD data were acquired in a suitable low-to-medium angle 2θ range. Then, the sample holders were introduced into an air-tight water-vapor saturated cells. At different time points, each sample was checked by PXRD, adopting the same conditions employed for the preliminary acquisitions.

Measurement of the Contact Angle: 1-mm thick pellets of [Ag_2(BTB)], FN-PCP-1, and FMOF-3 were prepared by pressing batches of the three materials at 0.5 kbar for 5 min. A drop of distilled water was then laid down the surface. A series of pictures was taken with a common camera and processed by the software ImageJ[88] to estimate the contact angle.

Measurement of the Dielectric Constant: The value of the real component of the dielectric constant of samples of FMOF-1, FMOF-3, and FN-PCP-1 pressed into pellets was assessed at room temperature by metal-insulator–metal parallel plate capacitance measurements at 2 V and in the frequency range 2–2 × 10^6 Hz with an Agilent E4980A Precision LCR Meter with an Agilent 16048A Test Leads connection to a custom-made sample-holder and measuring head (Officina Elettrotecnica di Tenno, Ponte Arche, Italy). The real component of κ was estimated as the ratio between the capacitance of the pellet and that of air, the latter measured after setting the same distance, among the capacitors, at which the capacitance of the pellet was measured. The instrument was calibrated each time it was switched on by measuring the dielectric constant of a 12 mm wide, 1 mm thick pellet of Teflon. As a representative example of the calibration procedure, we obtained κ = 1.903(5) (Figure S18, Supporting Information) versus κ = 1.9–2.1 reported in the literature.[11] Each measurement, on both Teflon and the title materials, was repeated five times on the same pellet, alternating one acquisition on the pellet to one on air. The pellets (12 mm wide, 1 mm thick) were prepared by pressing a sample of each material at 0.5 kbar for 5 min and were kept in a desiccator prior to measurement. The structural integrity of the pressed samples was verified by means of PXRD. In the case of FMOF-1, pelletization brings about amorphization (Figure S19, Supporting Information). To verify the dependence of κ on the degree of amorphization, pellets of FMOF-1 were prepared by pressing the material at different pressures (0.5 and 0.7 kbar) for 5 min. As for the measurements of the dielectric constant after pellet exposure to water vapor, prior to the measurements, the pellet was left 24 h in an air-tight cell at nearly saturated humidity levels.

High-Resolution Powder X-Ray Diffraction: High-resolution PXRD in situ and operando measurements were performed at the ID22 beamline of the European Synchrotron Radiation Facility (Grenoble, France). Samples of FMOF-3 and FN-PCP-1 were pressed into (1 mm thick, 0.6 mm wide) pellets at 0.5 kbar for 5 min. The pellets were sandwiched between two coverslips coated with indium-tin oxide (sheet resistance 5 Ω sq^{-1}) using conductive silver paint contacts. The sides of the cell were attached to a function generator (Fluke PM-5136); the applied voltage between the coverslips was measured via an oscilloscope. HR-PXRD data were acquired on the pellets in the absence of electric current and while applying an AC current of constant voltage (2 V) and different frequencies (in the 1–5 × 10^5 Hz range). Data were acquired at 31 keV (λ = 0.399 Å, calibrated with the Si NIST standard SRM 640c at room temperature), with a beam size of 1.0 × 1.0 mm^2 (FMOF-3) or 1.2 mm (horizontal) by 1.5 mm (vertical) (FN-PCP-1) defined by water-cooled slits and monochromated by a cryogenically cooled Si 111 channel-cut crystal. A bank of nine detectors, each preceded by a Si 111 analyzer crystal, was scanned vertically to measure the diffracted intensity. Rietveld refinements of the crystal structures were carried out with TOPAS-R using, as starting point, the crystal structure obtained at ambient conditions. For FN-PCP-1, peak shape anisotropy was described according to the model proposed by Stephens[86] for orthorhombic space groups using the Lorentzian contribution alone. Preferred orientation along the [101][89] crystallographic direction was corrected with the March-Dollase[90] model. For FMOF-3, the peak shape was described with a tan(θ)-dependent Lorentzian contribution diversified for the [00*l*] classes of reflections and the other ones. Preferred orientation along the [111] direction was corrected with the March-Dollase model. In both cases, the Bragg reflections belonging to Ag (from the silver paint) were modeled with the crystal structure of silver retrieved from the Inorganic Crystal Structure Database (ICSD code 604 631). Figure S12 of the Supporting Information collects the HR data measured for the two compounds at all the frequencies essayed, Figure S13 of the Supporting Information provides representative examples of Rietveld refinements, while Tables S1.1 and S1.2 compile the main crystallographic data and Rietveld refinement results.

Supporting Information

Supporting Information is available from the Wiley Online Library or from the author.

Acknowledgements

S.G., A.C., and J.F.I. contributed equally to this work. Under the supervision of A.M., A.C. carried out the synthesis and preliminary characterization (elemental analysis, infrared spectroscopy, thermogravimetric analysis) of H2BTB, H2FBTB, FN-PCP-1, FMOF-3, lc-[Cu(BTB)(DMF)], and [Ag2(BTB)]. Under the supervision of M.A.O.: a) J.F.I. and A.C. carried out the synthesis and characterization of FMOF-1 and measured the N2 adsorption isotherms for FN-PCP-1 and FMOF-3. b) J.F.I. carried out the synthesis and preliminary characterization of ZIF-8 and the calculation of the specific surface area of FMOF-3 with Materials Studio. c) M.R. measured the experimental contact angle on FN-PCP-1 and [Ag2(BTB)] and performed the thin film casting studies of FMOF-1 on low-carbon steel. d) R.A. measured the CO_2 adsorption isotherm on FMOF-3. e) C.C. performed the synthesis of the triazolate ligand. f) W.Y. performed the thin film casting studies of FMOF-1 on Si. Under the supervision of S.G.: a) C.G. unraveled the crystal structure of FN-PCP-1 and FMOF-3, carried out the VT-PXRD experiments on FN-PCP-1 and FMOF-3, and measured the dielectric constants of H2BTB, H2FBTB, FN-PCP-1, and FMOF-3. b) R.V. carried out the VT-PXRD experiment on FMOF-1, measured the dielectric constant of FMOF-1 and ZIF-8 and the experimental contact angle of FMOF-3, monitored the chemical stability of FMOF-1, FN-PCP-1, and FMOF-3. c) R.V., C.G., and S.C. carried out the experiment at ESRF and the successive data treatment. Finally, S.G. and M.A.O. contributed to the manuscript writing and editing, and corresponded with each other on data interpretation and manuscript decisions. The authors thank Prof. Bruce E. Gnade, Thomas R. Cundari, and Giovanni Palmisano for helpful discussions. The Galli group acknowledges the University of Insubria for partial funding. M.A.O. greatly acknowledges support of his group's contributions from the Welch Foundation (B-1542) and the U.S. National Science Foundation (CHE-1413641 for research support and CHE-1726652 for equipment support). The authors are also grateful to the European Synchrotron Radiation Facility (experiment CH-4795).

Conflict of Interest

The authors declare no conflict of interest.

Keywords

coordination polymers, fluorous metal–organic frameworks, fluorous nonporous coordination polymers, low-dielectric-constant materials, metal–organic frameworks

Received: June 12, 2019
Revised: July 10, 2019

---

[1] M. R. Baklanov, K. Vanstreels, C. Wu, Y. Li, K. Croes, in *Thin Films on Silicon: Electronic and Photonic Applications* (Eds: V. Narayanan, M. M. Frank, A. A. Demkov), World Scientific Publishing, Singapore, Taiwan **2017**, Ch. 5.

[2] P. S. Ho, J. Leu, W. W. Lee Eds., *Low Dielectric Constant Materials for IC Applications*, Springer Verlag, Berlin Heidelberg, Germany **2003**.

[3] W. Volksen, R. D. Miller, G. Dubois, *Chem. Rev.* **2010**, *110*, 56.

[4] W. C. Wang, R. H. Vora, E. Kang, K. G. Neoh, C. K. Ong, L. F. Chen, *Adv. Mater.* **2004**, *16*, 5457.

[5] S. J. Martin, J. P. Godschalx, M. E. Mills, E. O. Schaffer, P. H. Townsend, *Adv. Mater.* **2000**, *12*, 1769.

[6] D. Edelstein, J. Heidenreich, R. Goldblatt, W. Cote, C. Uzoh, N. Lustig, P. Roper, T. McDevitt, W. Motsiff, A. Simon, J. Dukovic, R. Wachnik, H. Rathore, R. Schulz, L. Su, S. Luce, J. Slattery, *Tech. Dig. Int. Electron. Devices Meet.* **1997**, *31-3*, 773.

[7] http://www.itrs2.net/, access date June 11th **2019**.

[8] By definition, low-κ; materials are materials with κ; < 4.

[9] P. Gonon, A. Sylvestre, H. Meynen, L. Van Cotthem, *J. Electrochem. Soc.* **2003**, *150*, F47.

[10] C.-C. Chiang, M.-C. Chen, L.-J. Li, Z.-C. Wu, S.-M. Jang, M.-S. Liang, *J. Electrochem. Soc.* **2004**, *151*, G612.

[11] F. W. Sears, M. W. Zemansky, H. D. Young, *University Physics*, 6th Ed., Addison-Wesley, Boston, MA **1982**.

[12] D. M. Smith, G. P. Johnston, W. C. Ackerman, S.-P. Jeng, B. E. Gnade, U.S. Pat. 6,437,007 B1, **2002**.

[13] D. M. Smith, G. P. Johnston, W. C. Ackerman, R. A. Stoltz, A. Maskara, T. Ramos, S.-P. Jeng, B. E. Gnade, U.S. Pat. 6,645,878 B2, **2003**.

[14] C.-C. Chiang, I.-H. Ko, M.-C. Chen, Z.-C. Wu, Y.-C. Lu, S.-M. Jang, M.-S. Liang, *J. Electrochem. Soc.* **2004**, *151*, G704.

[15] K. Zagorodniy, G. Seifert, H. Hermann, *Appl. Phys. Lett.* **2010**, *97*, 251905.

[16] E. Albanese, B. Civalleri, M. Ferrabone, F. Bonino, S. Galli, A. Maspero, C. Pettinari, *J. Mater. Chem.* **2012**, *22*, 22592.

[17] F. Wang, C. Y. Ni, Q. Liu, F. L. Li, J. Shi, H. X. Li, J. P. Lang, *Chem. Commun.* **2013**, *49*, 9248.

[18] H. Guo, M. Wang, J. Liu, S. Zhu, C. Liu, *Microporous Mesoporous Mater.* **2016**, *221*, 40.

[19] R. Warmbier, A. Quandt, G. Seifert, *J. Phys. Chem. C* **2014**, *118*, 11799.

[20] S. Mendiratta, M. Usman, T. T. Luo, S. F. Lee, Y. C. Lin, K. L. Lu, *CrystEngComm* **2014**, *16*, 6309.

[21] S. Mendiratta, M. Usman, T. T. Luo, B. C. Chang, S. F. Lee, Y. C. Lin, K. L. Lu, *Cryst. Growth Des.* **2014**, *14*, 1572.

[22] S.-S. Yu, G.-J. Yuan, H.-B. Duan, *RSC Adv.* **2015**, *5*, 45213.

[23] P. Yang, X. He, M. X. Li, Q. Ye, J. Z. Ge, Z. X. Wang, S. R. Zhu, M. Shao, H. L. Cai, *J. Mater. Chem.* **2012**, *22*, 2398.

[24] V. Di Noto, A. B. Boeer, S. Lavina, C. A. Muryn, M. Bauer, G. A. Timco, E. Negro, M. Rancan, R. E. P. Winpenny, S. Gross, *Adv. Funct. Mater.* **2009**, *19*, 3226.

[25] L. Z. Chen, J. Zou, Y. M. Gao, S. Wan, M. N. Huang, *J. Coord. Chem.* **2011**, *64*, 715.

[26] P. C. Guo, T. Y. Chen, X. M. Ren, W. H. Ning, W. Jin, *New J. Chem.* **2014**, *38*, 2254.

[27] W.-J. Li, J. Liu, Z.-H. Sun, T.-F. Liu, J. Lü, S.-Y. Gao, C. He, R. Cao, J.-H. Luo, *Nat. Commun.* **2016**, *7*, 11830.

[28] M. R. Ryder, Z. Zeng, K. Titov, Y. Sun, E. M. Mahdi, I. Flyagina, T. D. Bennett, B. Civalleri, C. S. Kelley, M. D. Frogley, G. Cinque, J.-C. Tan, *J. Phys. Chem. Lett.* **2018**, *9*, 2678.

[29] K. Titov, Z. Zeng, M. R. Ryder, A. K. Chaudhari, B. Civalleri, C. S. Kelley, M. D. Frogley, G. Cinque, J.-C. Tan, *J. Phys. Chem. Lett.* **2017**, *8*, 5035.

[30] C. Serre, *Angew. Chem., Int. Ed.* **2012**, *51*, 6048.

[31] C. Yang, X. Wang, M. A. Omary, *J. Am. Chem. Soc.* **2007**, *129*, 15454.

[32] P. Z. Moghadam, J. F. Ivy, R. K. Arvapally, A. M. dos Santos, J. C. Pearson, L. Zhang, E. Tyllianakis, P. Ghosh, I. W. H. Oswald, U. Kaipa, X. Wang, A. K. Wilson, R. Q. Snurr, M. A. Omary, *Chem. Sci.* **2017**, *8*, 3989.

[33] T.-H. Chen, I. Popov, O. Zenasni, O. Daugulis, O. S. Miljanić, *Chem. Commun.* **2013**, *49*, 6846.

[34] C. Yang, R. K. Arvapally, S. M. Tekarly, G. A. Salazar, O. Elbjeirami, X. Wang, M. A. Omary, *Angew. Chem., Int. Ed.* **2015**, *54*, 4842.

[35] C. Yang, M. A. Omary, U.S. Pat. 8,715,395, **2014**.

[36] C. Yang, M. A. Omary, U.S. Pat. 8,343,260, **2013**.

[37] N. Nijem, P. Canepa, U. Kaipa, K. T. K. Roodenko, S. M. Tekarli, J. Halbert, I. W. H. Oswald, R. K. Arvapally, C. Yang, T. Thonhauser, M. A. Omary, Y. J. Chabal, *J. Am. Chem. Soc.* **2013**, *135*, 12615.

[38] C. Yang, U. Kaipa, Q. Z. Mather, X. Wang, V. Nesterov, A. F. Venero, M. A. Omary, *J. Am. Chem. Soc.* **2011**, *133*, 18094.

[39] C. Yang, X. Wang, M. A. Omary, *Angew. Chem., Int. Ed.* **2009**, *48*, 2500.

[40] A. Tabacaru, S. Galli, C. Pettinari, N. Masciocchi, T. M. McDonald, J. R. Long, *CrystEngComm* **2015**, *17*, 4992.

[41] S. Galli, A. Maspero, C. Giacobbe, G. Palmisano, L. Nardo, A. Comotti, I. Bassanetti, P. Sozzani, N. Masciocchi, *J. Mater. Chem. A* **2014**, *2*, 12208.

[42] V. Colombo, C. Montoro, A. Maspero, G. Palmisano, N. Masciocchi, S. Galli, E. Barea, J. A. R. Navarro, *J. Am. Chem. Soc.* **2012**, *134*, 12830.

[43] E. Quartapelle Procopio, S. Rojas, N. M. Padial, S. Galli, N. Masciocchi, F. Linares, D. Miguel, J. E. Oltra, J. A. R. Navarro, E. Barea, *Chem. Commun.* **2011**, *47*, 11751.

[44] V. Colombo, S. Galli, H. J. Choi, G. D. Han, A. Maspero, G. Palmisano, N. Masciocchi, J. R. Long, *Chem. Sci.* **2011**, *2*, 1311.

[45] I. Stassen, N. Burtch, A. Talin, P. Falcaro, M. Allendorf, R. Ameloot, *Chem. Soc. Rev.* **2017**, *46*, 3185.

[46] M. Usman, S. Mendiratta, K.-L. Lu, *ChemElectroChem* **2015**, *2*, 786.

[47] M. D. Allendorf, A. Schwartzberg, V. Stavila, A. A. Talin, *Chem. - Eur. J.* **2011**, *17*, 11372.

[48] M. Usman, Kuang-Lieh Lu, *NPG Asia Mater.* **2016**, *8*, e333.

[49] S. Mendiratta, M. Usman, K.-L. Lu, *Coord. Chem. Rev.* **2018**, *360*, 77.

[50] S. Eslava, L. Zhang, S. Esconjauregui, J. Yang, K. Vanstreels, M. R. Baklanov, E. Saiz, *Chem. Mater.* **2013**, *25*, 27.

[51] M. Usman, C.-H. Lee, D.-S. Hung, S.-F. Lee, C.-C. Wang, T.-T. Luo, L. Zhao, M.-K. Wu, K.-L. Lu, *J. Mater. Chem. C* **2014**, *2*, 3762.

[52] J. J. Low, A. I. Benin, P. Jakubczak, J. F. Abrahamian, S. A. Faheem, R. R. Willis, *J. Am. Chem. Soc.* **2006**, *131*, 15835.

[53] L. Huang, H. Wang, J. Chen, Z. Wang, J. Sun, D. Zhao, Y. Yan, *Microporous Mesoporous Mater.* **2003**, *58*, 105.

[54] J. A. Greathouse, M. D. Allendorf, *J. Am. Chem. Soc.* **2006**, *128*, 10679.

[55] M. Dincă, A. F. Yu, J. R. Long, *J. Am. Chem. Soc.* **2006**, *128*, 8904.

[56] A. Maspero, S. Galli, V. Colombo, G. Peli, N. Masciocchi, S. Stagni, E. Barea, J. A. R. Navarro, *Inorg. Chim. Acta* **2009**, *362*, 4340.

[57] A. Maspero, S. Galli, N. Masciocchi, G. Palmisano, *Chem. Lett.* **2008**, *37*, 956.

[58] T.-H. Chen, I. Popov, W. Kaveevivitchai, Y.-C. Chuang, Y.-S. Chen, A. J. Jacobson, O. Š. Miljanić, *Angew. Chem., Int. Ed.* **2015**, *54*, 13902.

[59] Z. P. Demko, K. B. Sharpless, *J. Org. Chem.* **2001**, *66*, 7945.

[60] J. A. Joule, K. Mills, *Heterocyclic Chemistry*, 5th ed., Wiley-VCH, Hoboken, NJ **2010**.

[61] Estimated as the distance between the nearest fluorine atoms decorating opposite walls, taking into consideration the van der Waals radius of fluorine (S. S. Batsanov, *Inorg. Mater.* **2001**, *37*, 871).

[62] The empty volume was calculated with the software Platon (A. L. Spek, *Acta Crystallogr., Sect. D: Biol. Crystallogr.* **2009**, *65*, 148).

[63] W. M. Bloch, R. Babarao, M. R. Hill, C. J. Doonan, C. J. Sumby, *J. Am. Chem. Soc.* **2013**, *135*, 10441.

[64] Y. S. Bae, A. M. Spokoyny, O. K. Farha, R. Q. Snurr, J. T. Hupp, C. A. Mirkin, *Chem. Commun.* **2010**, *46*, 3478.

[65] Y. Hu, W. M. Verdegaal, S. H. Yu, H. L. Jiang, *ChemSusChem* **2014**, *7*, 734.

[66] Q. Yan, Y. Lin, C. Kong, L. Chen, *Chem. Commun.* **2013**, *49*, 6873.

[67] S. Henke, R. A. Fischer, *J. Am. Chem. Soc.* **2011**, *133*, 2064.

[68] Materials Studio v. 4.1, Biovia, San Diego, CA, USA.

[69] P. A. Kohl, *Annu. Rev. Chem. Biomol. Eng.* **2011**, *2*, 379.

[70] More in detail, in the same temperature range, the *a*-axis is essentially unaffected by temperature increase, whereas the *b*- and *c*-axis vary by –0.3% and 1.2%, with a consequent modification of the aperture of the 1-D channels.

[71] The radius of the circumference inscribed in the rhombic channel increases by ~1%.

[72] S. K. Henninger, F. P. Schmidt, H. M. Henning, *Adsorption* **2011**, *17*, 833.

[73] A drop of water laid down a pellet of lc-[Cu(BTB)(DMF)] occupies all the available surface, precluding contact angle measurements and suggesting a hydrophilic behaviour.

[74] N. M. Padial, E. Quartapelle Procopio, C. Montoro, E. López, J. E. Oltra, V. Colombo, A. Maspero, N. Masciocchi, S. Galli, I. Senkovska, S. Kaskel, E. Barea, J. A. R. Navarro, *Angew. Chem., Int. Ed.* **2013**, *52*, 8290.

[75] The dielectric constant of **FMOF-1** is higher when pressed at 0.5 kbar than when pressed at 0.7 kbar, which is counterintuitive, as high pressure reasonably causes a reduction in the air (κ;~1) volume contained in the pellet, which should increase κ;. This is completely correct only when considering *dry* air for a material with the same degree of crystallinity as a function of pressure. Despite the nominal superhydrophobic behaviour of **FMOF-1**, ref. [37] has shown by in situ vibrational spectroscopy that minute amounts of non-hydrogen-bonded water (albeit undetectable by adsorption isotherms, [38]nor GCMC simulations thereof [32]) are attached to the **FMOF-1** surface. Moreover, the phase purity of the material is compromised upon increasing the applied pressure to attain an increased admixture of amorphous material (Figure S19).

[76] In the case of **FMOF-1**, to obtain the corrected κ; values, the bulk density of the crystalline phase, not that of the amorphous one, was taken into consideration.

[77] K. S. Park, Z. Ni, A. P. Côté, J. Y. Choi, R. Huang, F. J. Uribe-Romo, H. K. Chae, M. O'Keeffe, O. M. Yaghi, *Proc. Natl. Acad. Sci. USA* **2006**, *103*, 10186.

[78] K. Jayaramulu, K. K. R. Datta, C. Rçsler, M. Petr, *Angew. Chem., Int. Ed.* **2016**, *55*, 1178.

[79] D. Bell, A. O. A. Eltoum, N. J. O'Reilly, A. E. Tipping, *J. Fluorine Chem.* **1993**, *64*, 151.

[80] M. M. Abdul-Ghani, A. E. Tipping, *J. Fluorine Chem.* **1995**, *72*, 95.

[81] R. A. Young, *The Rietveld Method*, IUCr Monograph N. 5, Oxford University Press, New York, USA, **1981**.

[82] TOPAS-R, version 3.0, Bruker, Karlsruhe, Germany, **2005**.

[83] For the rigid body describing the ligand, the following bond distances and angles have been adopted: C-N, N-N of the penta-atomic ring, 1.36 Å; C-C of the hexa-atomic ring, 1.39 Å; exocyclic C-C, refined in the range 1.40–1.50 Å (retrieved from a search for similar fragments within the 2019 update of the Cambridge Structural Database); C-F refined in the range 1.32–1.38 Å (retrieved from a search for aromatic C-F bonds within the 2019 update of the Cambridge Structural Database); penta-atomic ring internal bond angles, 108°; penta-atomic ring external bond angles, 126°; hexa-atomic ring bond angles, 120°. For the rigid body describing DMF, the following bond distances and angles have been adopted: C-N, 1.40 Å; C-H, 0.95 Å; C-O, 1.25 Å; angles at the N and aldehydic C atoms, 120°; angles at the methyl C atoms, 109.5°.

[84] R. W. Cheary, A. A. Coelho, *J. Appl. Crystallogr.* **1992**, *25*, 109.

[85] P. W. Stephens, *J. Appl. Crystallogr.* **1999**, *32*, 281.

[86] G. W. Stinton, J. S. O. Evans, *J. Appl. Crystallogr.* **2007**, *40*, 87.

[87] S. Brunauer, P. H. Emmett, E. Teller, *J. Am. Chem. Soc.* **1938**, *60*, 309.

[88] "ImageJ." *National Institutes of Health*, U.S. Department of Health and Human Services, imagej.nih.gov/ij/ (accessed June 11th 2019).

[89] The obtained value of *g*, 1.4, is compatible with the formation of platelets (T. Ida, *Adv. Ceram. Res. Center Ann. Rep.* **2013**, 2, 7) normal to the [101]direction upon pressing the material into pellets.

[90] W. A. Dollase, *J. Appl. Crystallogr.* **1986**, *19*, 267.